Progress In Electromagnetics Research M, Vol. 109, 89–100, 2022

A Simple Approach to Characterize a Buried Object under the Ground

Vasil Tabatadze[1], Kamil Karaçuha[2, *], Ömer F. Alperen[1], Sulayman Joof[2], and Revaz Zaridze[3]

Abstract—This study provides an alternative and straightforward approach to determining buried dielectric objects underground by employing the method of auxiliary sources. In the direct scattering problem, the Brewster angle is determined, and then the electromagnetic properties of the ground are determined. Later, the scattered field above the ground due to the buried object is evaluated. The localization of the buried object is obtained by the continuity of the field components while solving the inverse problem. The numerical experiments are done, and outcomes of the numerical experiments are compared with a commercial full-wave computational electromagnetic software. The outcomes reveal less than 1% deviation between the proposed approach and the commercial tool.

1. INTRODUCTION

For many decades, determining the existence and predicting the physical properties of an object or obstacle located unreachable or buried region has been one of the triggering desires for electrical engineers [1–3]. Such problems are called "*inverse problems*". Primarily, inverse problems cover imaging, mining, structuring, detection, analysis, and characterization of materials. Numerous methodologies are developed, and extensive research is conducted to achieve these two goals. The importance of the subject is to obtain such information by noninvasive approaches. In general, electromagnetic waves are employed since the waves can propagate through the media [4]. The reflection and scattering of the electromagnetic waves from discontinuities and edges lead to obtaining information from the region of interest. Previously, buried pipe monitoring based on the joint use of finite-difference time-domain method (FDTD) numerical modeling and linear tomographic inversion methods was investigated [5]. Besides, both two and three-dimensional problems for a buried object under a rough surface were analyzed by analytical and numerical approaches [6, 7]. In these studies, first, Green's function of the corresponding problem was obtained. Then, analytical and numerical analyses were provided. There are many different analytical and numerical approaches regarding the inverse problem. However, in the present study, the Method of Auxiliary Sources is employed to investigate the determination of an object buried underground [4, 8–10]. A two-dimensional ring was investigated previously in [4], and the comparison was made with analytical outcomes. In [8–10], the localization and physical characterization of buried objects were analyzed. In [11], Brewster angle approach was included to detect the buried object. Besides, the buried object under a rough surface was investigated in [2].

The present study addresses how to obtain the physical characteristics of the unknown buried object underground. To achieve this goal, a practical and novel approach is proposed. The first outcomes of the corresponding study were presented in [12]. However, [12] has only briefly covered the direct scattering of the same problem. The main achievement of the present study is to determine the Brewster Angle

Received 12 January 2022, Accepted 17 March 2022, Scheduled 29 March 2022

* Corresponding author: Kamil Karaçuha (karacuha17@itu.edu.tr).

[1] Informatics Institute, Istanbul Technical University, Istanbul, Turkey. [2] Department of Electrical Engineering, Istanbul Technical University, Istanbul, Turkey. [3] The Laboratory of Applied Electrodynamics, Tbilisi State University, Tbilisi, Georgia.

numerically, deduce the dielectric properties of the ground and then localize and characterize the buried object by a reflected field, including the inverse problem approach in the method of auxiliary sources (MAS) [9]. In the solution of the problem, there exist two main assumptions. The space is assumed to be two half-spaces, and the interface is flat. Then, the buried object is considered homogeneous, isotropic, linear, and simple dielectrics. It is better to summarize the approach before presenting the details. First, the Brewster angle of the interface is obtained by minimizing the reflected field where there is no buried object. Later, the characterization of the earth is obtained. Then, for the different frequencies, the region of interest is investigated. Note that the incident wave is sent from the Brewster angle. The frequency characteristics of the reflected field differ regarding the shape and physical characteristics of the object [12]. Finally, the localization of the object is obtained by the inverse scattering approach. By analytical continuity of the field, the position of the buried object is determined.

The present study first investigates the theoretical background in Section 2, and the numerical experimental outcomes are presented in Section 3. Then, the conclusion is provided in Section 4.

2. FORMULATION OF THE METHODOLOGY

2.1. Direct Problem

This section covers the mathematical background of the direct problem. In Fig. 1, the geometry of the problem is given. Surfaces S and S_1 stand for the physical interfaces of the layers and buried object, respectively. The prima notation corresponds to the auxiliary sources. As it is known, the fields in a different region can be expressed in terms of the corresponding auxiliary sources [12, 13]. Here, Region I is the free-space; Region II stands for the ground; and finally, Region III corresponds to the buried object. Auxiliary sources on S'' represent the field in Region I, whereas auxiliary sources on S' create the field in Region II. By shifting the sources, the singularity problem on the actual surface while applying the boundary condition is eliminated [14]. The same approach is employed in the buried object [15–17]. It should be noted that as the incident field, an H-polarized plane wave is used, and $e^{-i\omega t}$ is taken into account for the time convention where ω stands for the angular frequency.

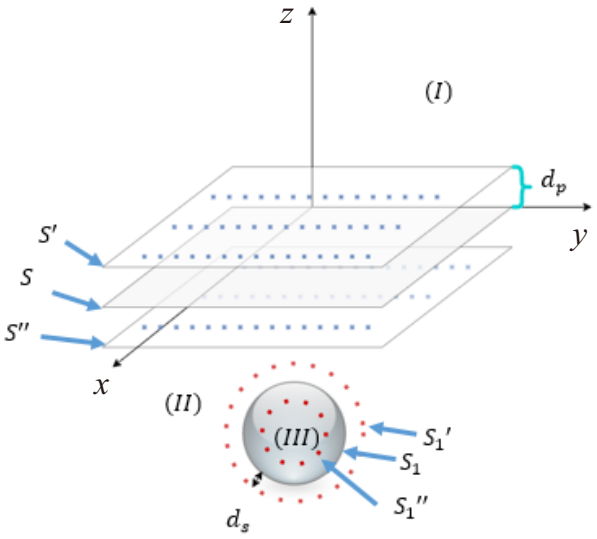

Figure 1. The geometry of the problem.

Shifting is defined by the following parameters: d_p and d_s for the corresponding interface to minimize the error. Since the auxiliary surfaces for each region define surfaces shifted from the actual surface, such parameters (d_p and d_s) correspond to the shifting of auxiliary surfaces from the physical interfaces, and they are important for obtaining accurate results. To express field components in three-dimensional space, a set of two orthogonal Hertzian dipoles are located to represent the scattered

field on the auxiliary surface. The combined field due to these Hertzian dipoles is given in Eqs. (1) and (2) [12, 18].

$$\vec{E}_{comb} = \vec{E}_{el} + \sqrt{\frac{\mu}{\epsilon}}\vec{E}_{mag} \tag{1}$$

$$\vec{H}_{comb} = \vec{H}_{el} + \sqrt{\frac{\mu}{\epsilon}}\vec{H}_{mag} \tag{2}$$

where

$$\vec{E}_{el} = \left(\frac{e^{ikR}}{4\pi\epsilon}\right)\left\{\left(\frac{1}{R^3} - \frac{ik}{R^2}\right)\left[3\vec{R}_0 \cdot \left(\vec{R}_0 \cdot \vec{p}_{el}\right) - \vec{p}_{el}\right] - \left(\frac{k^2}{R}\right)\left(\vec{R}_0 \times \left(\vec{R}_0 \times \vec{p}_{el}\right)\right)\right\},$$

$$\vec{E}_{mag} = \sqrt{\frac{\mu}{\epsilon}}\left(\frac{k^2 e^{ikR}}{4\pi}\right)\left(\frac{1}{R^2} - \frac{ik}{R}\right)\left(\vec{p}_{mag} \times \vec{R}_0\right),$$

$$\vec{H}_{el} = \left(\frac{i\omega e^{ikR}}{4\pi}\right)\left(\frac{1}{R^2} - \frac{ik}{R}\right)\left(\vec{R}_0 \times \vec{p}_{el}\right),$$

and,

$$\vec{H}_{mag} = \left(\frac{e^{ikR}}{4\pi\epsilon}\right)\left\{\left(\frac{1}{R^3} - \frac{ik}{R^2}\right)\left[3\vec{R}_0 \cdot \left(\vec{R}_0 \cdot \vec{p}_{mag}\right) - \vec{p}_{mag}\right] - \left(\frac{k^2}{R}\right)\left(\vec{R}_0 \times \left(\vec{R}_0 \times \vec{p}_{mag}\right)\right)\right\}.$$

Here [16, 19],

- $\vec{E}_{el}$ — Electric field vector of an electric dipole.
- $\vec{E}_{mag}$ — Electric field vector of the magnetic dipole.
- $\vec{H}_{el}$ — Magnetic field vector of the electric dipole.
- $\vec{H}_{mag}$ — Magnetic field vector of the magnetic dipole.
- ε — Permittivity.
- μ — Magnetic permeability.
- $\vec{R}_0$ — The unit vector from the source point to the observation point.
- R — The distance between the source and the observation point.
- $\vec{p}$ — Polarization vector of the dipole.
- $\times$ — Cross product

For each region (see Fig. 1), the electric and magnetic fields should be expressed mathematically. In Eqs. (3) and (4), the fields for Region I are provided.

$$\vec{E}_{(\mathrm{I})} = \vec{E}_{inc} + \sum_{n=1}^{N}\left(a_n\vec{E}^{(\mathrm{I})}_{comb} + b_n\vec{E}^{'(\mathrm{I})}_{comb}\right)_{S''} \tag{3}$$

$$\vec{H}_{(\mathrm{I})} = \vec{H}_{inc} + \sum_{n=1}^{N}\left(a_n\vec{H}^{(\mathrm{I})}_{comb} + b_n\vec{H}^{'(\mathrm{I})}_{comb}\right)_{S''} \tag{4}$$

Here, N stands for the number of collocation points, and the points are lying on S'' surface. Note that, for each point, there are two perpendicularly located Hertzian dipoles.

The fields in Region II are presented as Eqs. (5) and (6), respectively.

$$\vec{E}_{(\mathrm{II})} = \sum_{n=1}^{N}\left(c_n\vec{E}^{(\mathrm{II})}_{comb} + d_n\vec{E}^{'(\mathrm{II})}_{comb}\right)_{S'} + \sum_{m=1}^{N_0}\left(e_m\vec{E}^{(\mathrm{II})}_{comb} + f_m\vec{E}^{'(\mathrm{II})}_{comb}\right)_{S''_1} \tag{5}$$

$$\vec{H}_{(\mathrm{II})} = \sum_{n=1}^{N}\left(c_n\vec{H}^{(\mathrm{II})}_{comb} + d_n\vec{H}^{'(\mathrm{II})}_{comb}\right)_{S'} + \sum_{m=1}^{N_0}\left(e_m\vec{H}^{(\mathrm{II})}_{comb} + f_m\vec{H}^{'(\mathrm{II})}_{comb}\right)_{S''_1} \tag{6}$$

Here, the fields in Region III are given below:

$$\vec{E}_{(\mathrm{III})} = \sum_{m=1}^{N_0} \left(e_m \vec{E}_{comb}^{(\mathrm{III})} + f_m \vec{E}_{comb}^{'(\mathrm{III})} \right)_{S_1'} \tag{7}$$

$$\vec{H}_{(\mathrm{III})} = \sum_{m=1}^{N_0} \left(e_m \vec{H}_{comb}^{(\mathrm{III})} + f_m \vec{H}_{comb}^{'(\mathrm{III})} \right)_{S_1'} \tag{8}$$

To obtain unknown coefficients $(a_m, b_m, c_m, d_m, e_m, f_m)$, the boundary conditions on each surface should be satisfied as:

$$\begin{aligned} \left(\vec{E}_{(\mathrm{I})} \cdot \vec{\tau}\right)\Big|_S &= \left(\vec{E}_{(\mathrm{II})} \cdot \vec{\tau}\right)\Big|_S, \quad \left(\vec{E}_{(\mathrm{II})} \cdot \vec{\tau}\right)\Big|_{S_1} = \left(\vec{E}_{(\mathrm{III})} \cdot \vec{\tau}\right)\Big|_{S_1} \\ \left(\vec{H}_{(\mathrm{I})} \cdot \vec{\tau}\right)\Big|_S &= \left(\vec{H}_{(\mathrm{II})} \cdot \vec{\tau}\right)\Big|_S, \quad \left(\vec{H}_{(\mathrm{II})} \cdot \vec{\tau}\right)\Big|_{S_1} = \left(\vec{H}_{(\mathrm{III})} \cdot \vec{\tau}\right)\Big|_{S_1} \end{aligned} \tag{9}$$

where $\vec{\tau}$ stands for the corresponding tangential vector on each physical surface.

Before ending, there are $4[N + N_0]$ unknowns in the system. The boundary conditions given in Eq. (9) are employed to obtain the unknowns. Then, a matrix system of linear algebraic equations is achieved. By matrix inversion, the unknown coefficients are determined.

To find the Brewster angle (θ_B), Eq. (10) is utilized.

$$\tan\theta_B = \sqrt{\frac{\epsilon_2}{\epsilon_1}} \tag{10}$$

Here, ϵ_1 and ϵ_2 are two different relative permittivities of upper and lower half-spaces, respectively.

Fresnel formula for parallel (H) polarization [20]

$$\Gamma_{||} = \frac{-\sqrt{\frac{\mu_1}{\epsilon_1}}\cos\theta_i + \sqrt{\frac{\mu_2}{\epsilon_2}}\cos\theta_t}{\sqrt{\frac{\mu_1}{\epsilon_1}}\cos\theta_i + \sqrt{\frac{\mu_1}{\epsilon_1}}\cos\theta_t} \tag{11}$$

where θ_i is the incident angle, and θ_t is the transmitted angle. The incident and transmitted angles are measured on the z-x plane from the z-axis. As a source of the incident wave, we have a Hertzian dipole located at the far-zone (100 meters radius from the origin, more than 10 wavelengths is assumed for the lowest frequency in the investigation as the far-field), and the magnetic field component is in the y-axis.

2.2. Inverse Problem

In this subsection, the theoretical background of the inverse problem is presented. The main advantage of the proposed method is that it can be employed even when the wavelength is comparable to the size of the scatterer [21]. To obtain the field expression underground, the property, including the continuation of the field, is taken into account. The buried object image reconstruction utilizing the reflected field above the ground is investigated in this part. It should be repeated that the object is a dielectric object and has its resonance characteristics depending on its physical and electrical properties. In Fig. 2, the geometry of the inverse problem is presented. Here, d_{sen} and d_{aux} are the amounts of the shift of sensors (receiving antenna system) and auxiliary sources from the corresponding physical surface, respectively. Below, the yellow region is the reconstruction region of interest. The following formula gives the reconstructed field distribution on the surface of the auxiliary sources:

$$\vec{E}_{rec}(\vec{r}) = \sum_{i=1}^{N_1 \times N_1} A_i G\left(-k\left|\vec{r} - \vec{r}'\right|\right) \cdot \vec{\tau}_x + \sum_{i=1}^{N_1 \times N_1} B_i G\left(-k\left|\vec{r} - \vec{r}'\right|\right) \cdot \vec{\tau}_y \tag{12}$$

where

$$G = \left(\frac{e^{ikR}}{4\pi\epsilon}\right)\left\{\left(\frac{1}{R^3} - \frac{ik}{R^2}\right)\left[3\vec{R}_0 \cdot \left(\vec{R}_0 \cdot \vec{p}_{el}\right) - \vec{p}_{el}\right] - \left(\frac{k^2}{R}\right)\left(\vec{R}_0 \times \left(\vec{R}_0 \times \vec{p}_{el}\right)\right)\right\}$$

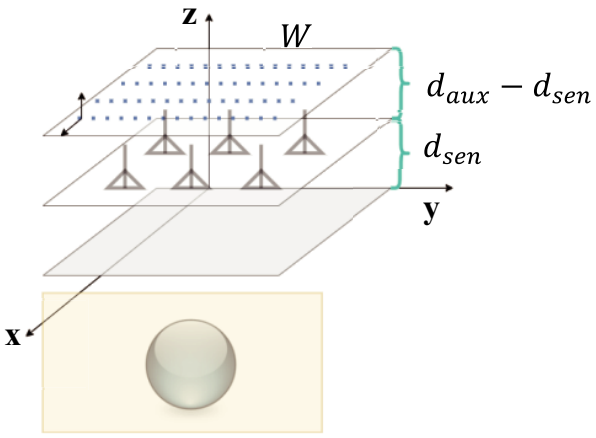

Figure 2. The sensors and the object locations.

It should be highlighted that $(-k|\vec{r}-\vec{r}'|)$ in Eq. (12) corresponds to the incoming waves to the sensors for the reconstruction of the field since the reconstructed field at the auxiliary surface ($S_{aux} = d_{aux}$) can be modeled as the incoming waves, not the outcoming waves. Due to analytical continuity:

$$\vec{E}_{rec}\left(\vec{r}\right)\cdot\vec{\tau}_x\Big|_{S_{aux}} = \vec{E}_{meas}\left(\vec{r}\right)\cdot\vec{\tau}_x\Big|_{S_{aux}}$$
$$\vec{E}_{rec}\left(\vec{r}\right)\cdot\vec{\tau}_y\Big|_{S_{aux}} = \vec{E}_{meas}\left(\vec{r}\right)\cdot\vec{\tau}_y\Big|_{S_{aux}}$$

where $\vec{E}_{meas}$ is obtained by the direct problem given in the previous section.

As noted, Green's function in Eq. (12) contains the information on the dielectric permittivity of the corresponding region. In layered media, the following definition of the permittivity expression is employed to have an approximate (average value) permittivity for the entire space [22]:

$$\epsilon_{reff} = \frac{\epsilon_r^{\text{ground}}+1}{2} + \frac{\epsilon_r^{\text{ground}}-1}{2}\left[1+12\frac{h}{W}\right]^{-\frac{1}{2}} \tag{13}$$

where h is equal to d_{aux}, and W is the width of the auxiliary surface. It should be highlighted that this formula is valid under the condition of $W \gg h$.

3. RESULTS OF NUMERICAL EXPERIMENTS

First, to find the Brewster angle between the air and ground with unknown dielectric permittivity, and the grid search is done between angles 0 and $\pi/2$. Obtaining the minimum reflected field gives the Brewster angle for such problems. Then, automatically, the real part of the relative dielectric constant is obtained. To determine the Brewster angle, 1 GHz is employed as the incidence field. It should be highlighted that throughout the study, only x-component of the electric field is considered due to having a TE polarization case. Also, for such problems, generally, linearly polarized antennas are used, and to be more realistic, one direction of the electric field is considered during direct and inverse problems.

3.1. Direct Problem

In this subsection, the numerical results regarding the direct problem are given. Before representing the numerical outcomes, it is better to give the parameters and dimensions in Table 1.

In Fig. 3, the amplitude of the ratios of the reflected field and incident field for different values of conductivity (σ) is presented. (R) is defined as the ratio of the absolute values of the reflected and incident electric fields. Here, the real value of the relative permittivity of the ground is taken as 4. Note that the theoretical Brewster angle can be found by Eq. (10), and its value is 63.435 in degree. However, the proposed methodology obtains the Brewster angle as 62.91 in degree which is used in the

Table 1. Location, dimensions (meter = m) and physical properties.

Center of Sphere	$(0, 0, -0.3)$ m	d_p	± 0.10 m
Center of Mine	$(0, 0, -0.3)$ m	d_s	± 0.035(sphere), ± 0.01(mine) m
Center of Cylinder	$(0, 0, -0.6)$ m	Height (cylinder)	0.4 m
ϵ_r(sphere)	6	Radii	15 cm (sphere), 8 cm (cylinder)
ϵ_r(mine)	6	Dimensions of Mine	0.2 m × 0.2 m × 0.1 m with a curvature radius at the corners 0.02 m

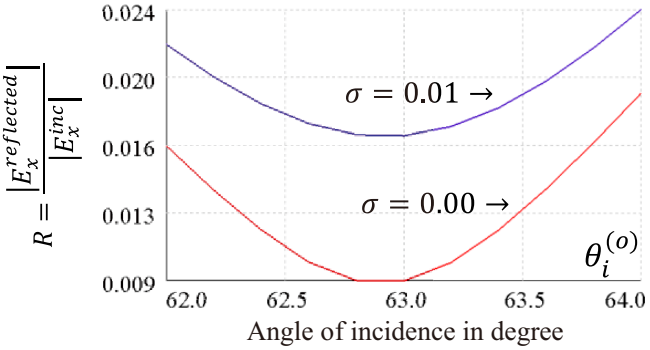

Figure 3. The ratio (R) of the absolute values of the reflected and the incident electric field for lossless ($\sigma = 0$) and lossy cases ($\sigma = 0.01$) versus incident angle in degree.

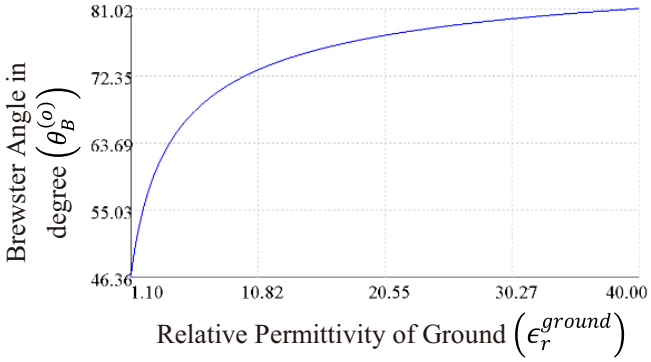

Figure 4. Brewster angle in degree versus the real part of $\epsilon_r^{\text{ground}}$.

numerical results. By obtaining the Brewster angle accurately, the unknown dielectric permittivity of the ground can be calculated by Eq. (10). The proposed approach obtains more diminutive than a 5% deviation from the exact values of the relative permittivity of the unknown ground. If the family of the graphs including different conductivities of the corresponding ground is calculated, the real value of the conductivity can be found by comparing previous outcomes.

In Fig. 4, the Brewster angle (θ_B) investigation for the ground with different relative permittivities is done. In Fig. 5, the convergence of the field is studied. To speed up the computation, the dimensions of both half-spaces should be minimized. Therefore, the amplitude of the x-component of the electric field distributions for different dimensions of the S area is investigated. As it is seen, the total physical surface S is assumed $7\lambda \times 7\lambda$ for the corresponding frequency since the deviation between two solutions is less than 1%. Therefore, the dimensions in Fig. 5(a) for the S surface are employed throughout the study. The conductivity (σ) of the buried object and the ground is taken as 0 for the following figures.

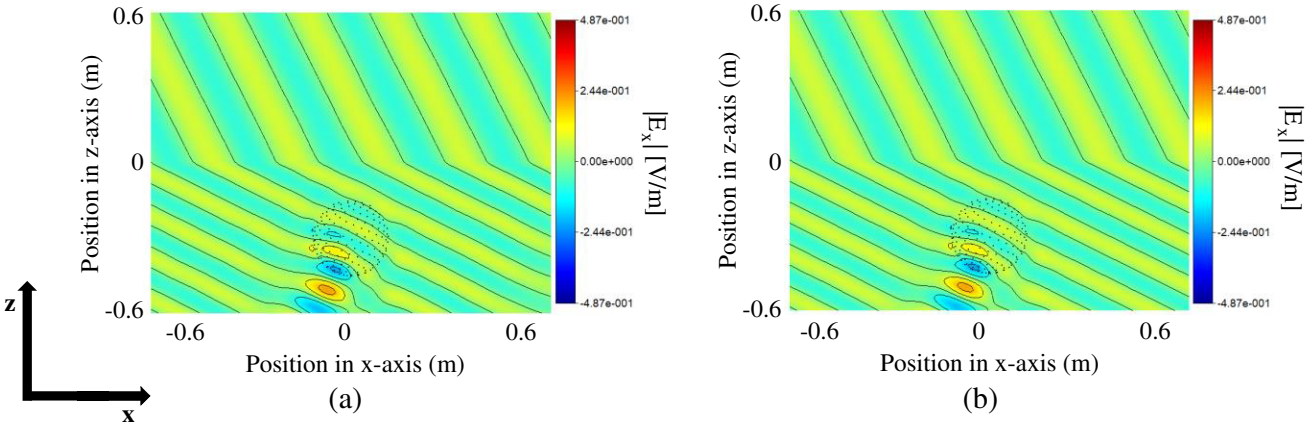

Figure 5. The comparison of the fields for different dimensions of S: (a) $7\lambda \times 7\lambda$, (b) $20\lambda \times 20\lambda$ at 1 GHz.

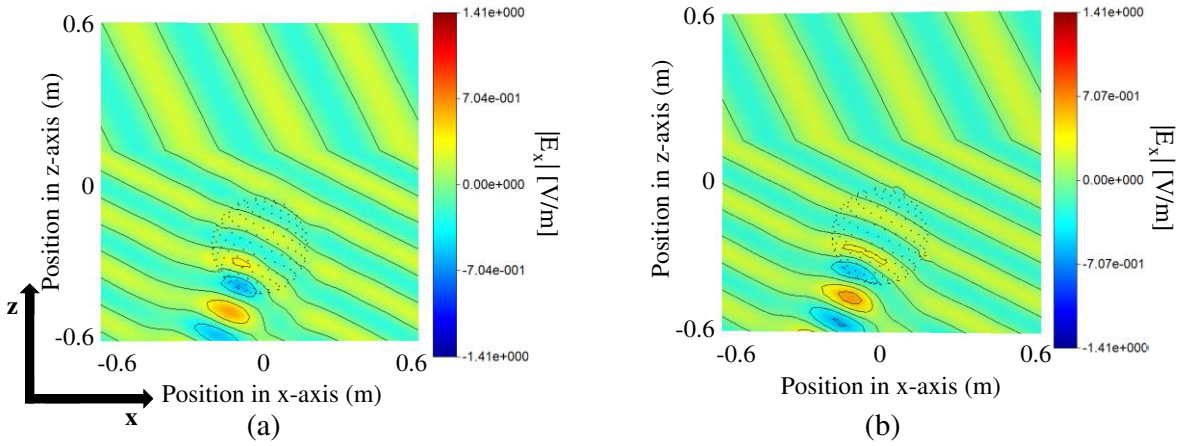

Figure 6. The comparison of the fields with (a) the proposed method and (b) FEKO computational electromagnetics software at 1 GHz.

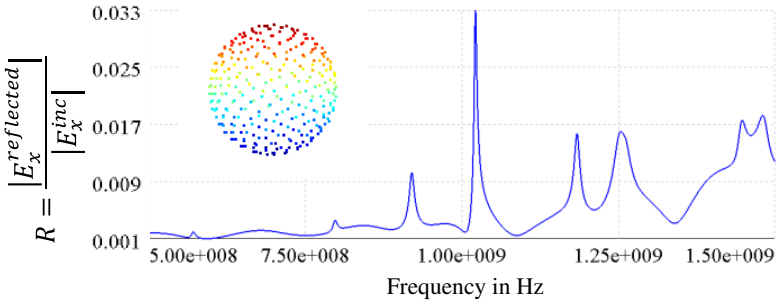

Figure 7. Frequency characteristics for $\epsilon_r^{\text{ground}} = 4$, $\epsilon_r^{\text{object}} = 6$, $\theta_{inc} = 63^\circ$ (sphere).

In Fig. 6, the comparison of the amplitude of the x-component of the electric field distributions is provided. The deviation is less than 1%. The deviation comes from the upper-right part of the obstacle. It should be noted that the proposed approach takes 1 minute to calculate the result, whereas with the same accuracy, Feldberechnung für körper mit beliebiger oberfläche (FEKO) computes in 30 minutes *(Properties of computer: Intel(R) Core(TM) i7-8700K CPU @ 3.70 GHz and installed RAM 32.0 GB).*

Figures 7–9 present the frequency characteristics of different objects. While obtaining these figures,

the amplitude of the scattered field at the point ($r_{obs} = (-\sin\theta_B, 0, \cos\theta_B)$) is drawn for a given frequency range as it is seen that the characteristics of these three figures are entirely different. When the buried object is a sphere, the resonances become narrow in a frequency band, and the peaks are close to each other. On the other hand, for the rectangular mine, the resonances are broad. In Fig. 7, the resonances characteristics of a cylinder shape are presented where the behavior is entirely different from the previous ones. This fact leads us to have the ability to distinguish buried objects with different shapes and dimensions.

In Figs. 10, 11, and 12, the amplitude of E_x is provided. For the lower half-space, the total E_x is presented, whereas only the reflected field is provided for the upper half-space to distinguish field characteristics easily when the buried object is in resonance. As can be seen in figures, there exists a

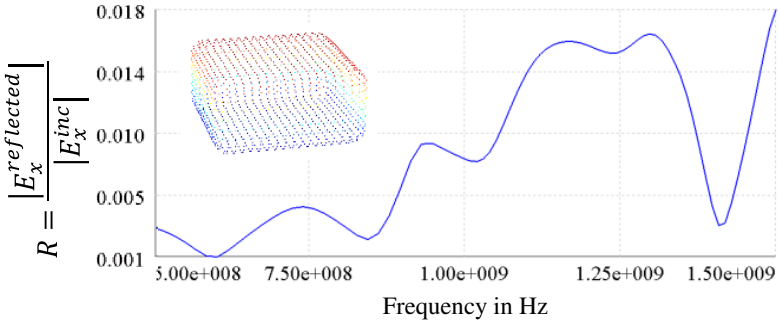

Figure 8. Frequency characteristics for $\epsilon_r^{\text{ground}} = 4$, $\epsilon_r^{\text{object}} = 6$, $\theta_{inc} = 63^\circ$ (rectangular mine).

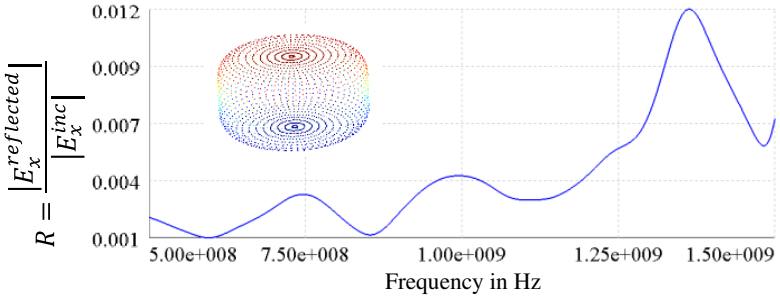

Figure 9. Frequency characteristics for $\epsilon_r^{\text{ground}} = 4$, $\epsilon_r^{\text{object}} = 6$, $\theta_{inc} = 63^\circ$ (cylinder).

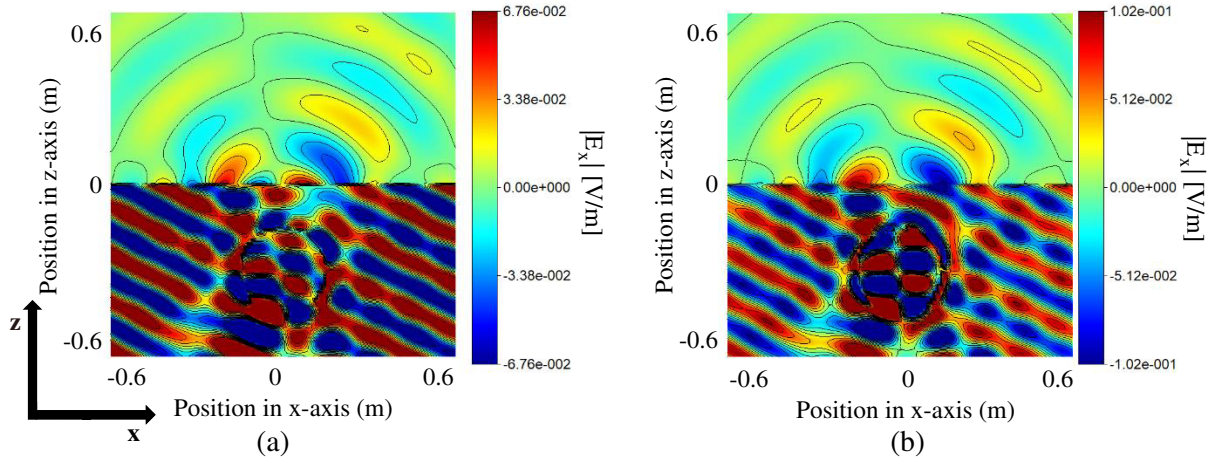

Figure 10. The amplitude of E_x in when the sphere is in resonance ($\epsilon_r^{\text{object}} = 6$, $\epsilon_r^{\text{ground}} = 4$), (a) 1.019 GHz, (b) 1.022 GHz.

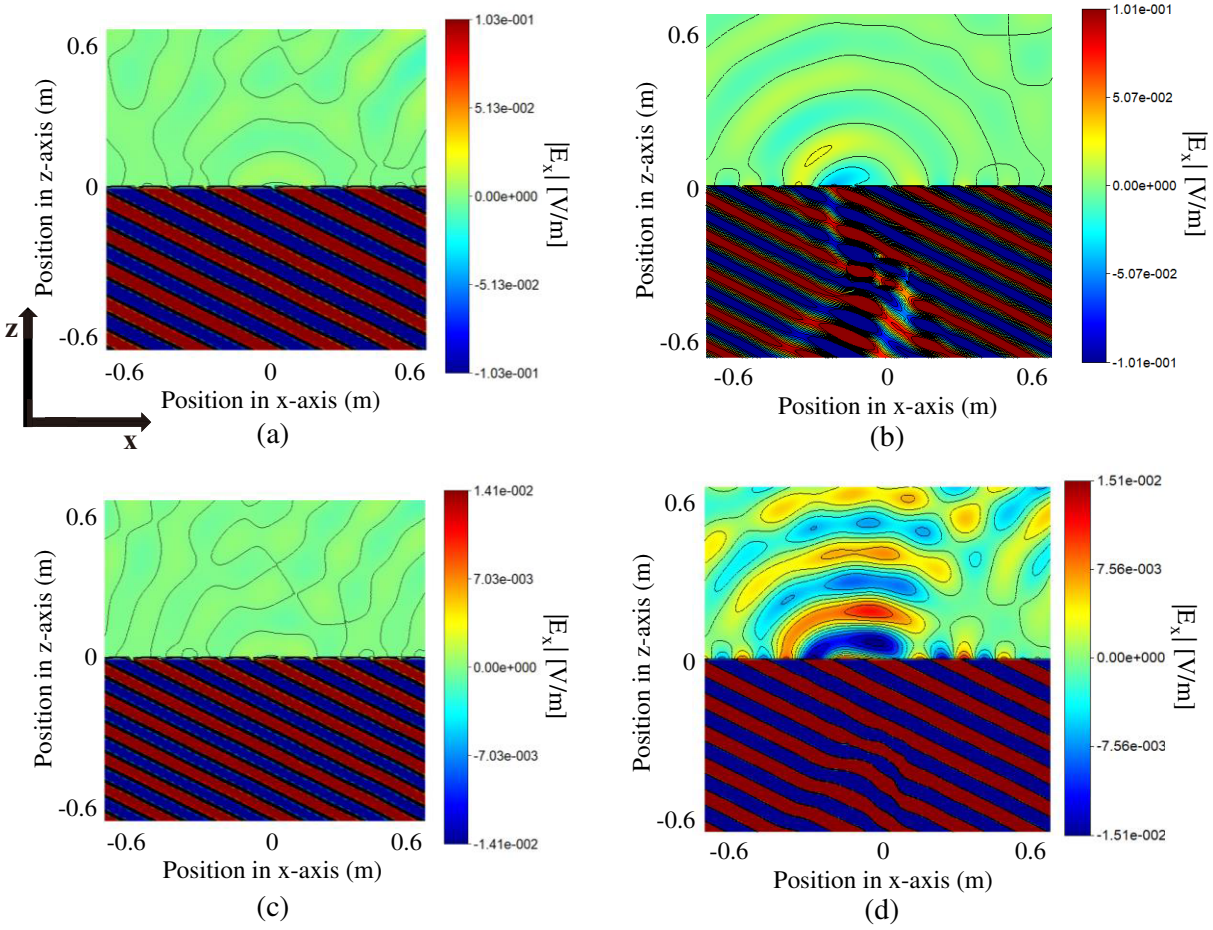

Figure 11. The amplitude of E_x ($\epsilon_r^{\text{mine}} = 6$, $\epsilon_r^{\text{ground}} = 4$), (a) no object at 1.3 GHz, (b) with the object at 1.3 GHz, (c) no object at 1.5 GHz, (d) with the object at 1.5 GHz.

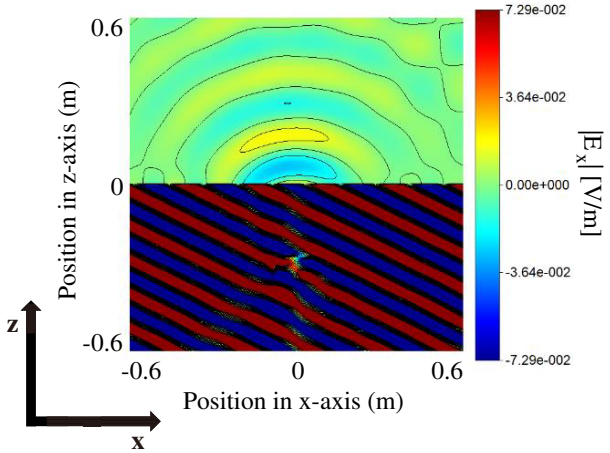

Figure 12. The amplitude of E_x ($\epsilon_r^{\text{cylinder}} = 6$, $\epsilon_r^{\text{ground}} = 4$) at 1.363 GHz (resonance).

noticeable change in the reflected field above the ground when the object is in resonance. Otherwise, the reflected field is negligible.

3.2. Inverse Problem

In this subsection, the numerical results regarding the inverse problem are provided. Before representing the numerical outcomes, it is better to give the parameters and dimensions in Table 2.

Table 2. Location, dimensions (in meter), and physical properties.

d_{sen}	0.1 meter	d_{aux}	0.2 meter
Number of Sensors	24×24 (2×2 meter^2 area)	frequencies	1.0, 1.3, 1.7 GHz

In Fig. 13, the reconstructed images of the buried object for the different cases are provided. The results reveal that employing Eq. (13) results in better localization of the reconstructed image. By Eq. (13), the effective relative permittivity of the regions is found 3.686. In reconstruction, the near field is obtained by employing Eq. (12) for three frequencies listed in Table 2. Here, only the absolute value of the x component of the electric field is utilized.

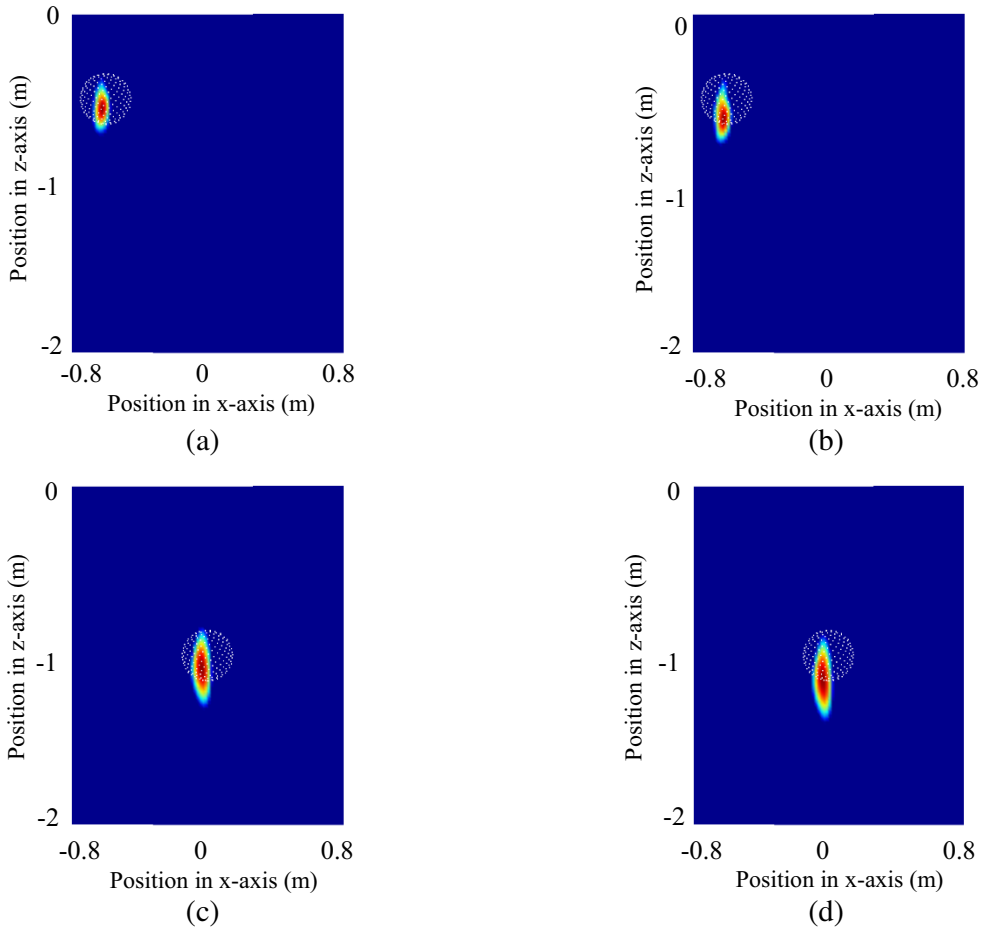

Figure 13. The reconstructed image of the buried sphere (a) located at $(-0.6, 0, -0.5)$ with ϵ_{eff}, (b) located at $(-0.6, 0, -0.5)$ with $\epsilon_r^{\text{ground}}$, (c) located at $(0, 0, -1)$ with ϵ_{eff}, (d) located at $(0, 0, -1)$ with $\epsilon_r^{\text{ground}}$.

4. CONCLUSION

The main aim is to propose a novel and simple solution to the direct and inverse electromagnetic scattering by three-dimensional dielectric geometries buried inside the ground. Here, MAS is used to determine the direct and inverse problems. The plane wave at the Brewster angle between two media is employed to achieve this goal. Three different geometries are considered, and the resonance characteristics of these corresponding geometries differ noticeably, leading to the discrimination of the geometries buried underground. After determining the object's shape by frequency characteristics, the inverse problem is solved to find the buried object's location. Here, effective permittivity is employed to localize better. The comparison between MAS and commercial program FEKO is utilized. Less than 1% deviation is observed.

ACKNOWLEDGMENT

The paper's authors would like to express their gratitude to the National Center for High-Performance Computing (UHEM) at Istanbul Technical University for access. This work is supported in part by Istanbul Technical University (ITU) Vodafone Future Lab under Project No. ITUVF20180901P10.

REFERENCES

1. Karaçuha, E., "Ters saçılma problemlerinde born yaklaşımıyla sağlanan eksik datanın Ramm fonksiyonu aracılığıyla analitik devamı," 1990 (in Turkish).
2. Altuncu, Y., I. Akduman, and A. Yapar, "Detecting and locating dielectric objects buried under a rough interface," *IEEE Geosci. Remote Sens. Lett.*, Vol. 4, No. 2, 251–255, 2007.
3. Idemen, M. and A. Alkumru, "On an inverse source problem connected with photo-acoustic and thermo-acoustic tomographies," *Wave Motion*, Vol. 49, No. 6, 595–604, 2012.
4. Tabatadze, V., K. Karaçuha, and E. Karaçuha, "Body shape and complex permittivity determination using the method of auxiliary sources," *Progress In Electromagnetics Research M*, Vol. 87, 115–125, 2019.
5. Millington, T. M., N. J. Cassidy, L. Crocco, and F. Soldovieri, "Tomographic GPR imaging using a linear inversion algorithm informed by FDTD modelling: A numerical case study of buried utility pipes monitoring," *Near Surf. Geophys.*, Vol. 11, No. 2, 221–230, 2013.
6. Altuncu, Y., A. Yapar, and I. Akduman, "On the scattering of electromagnetic waves by bodies buried in a half-space with locally rough interface," *IEEE Trans. Geosci. Remote Sens.*, Vol. 44, No. 6, 1435–1443, 2006.
7. Tetik, E. and I. Akduman, "3D imaging of dielectric objects buried under a rough surface by using CSI," *Int. J. Antennas Propag.*, Vol. 2015, 2015.
8. Shubitidze, F., et al., "Application of the normalized surface magnetic charge model to UXO discrimination in cases with overlapping signals," *J. Appl. Geophys.*, Vol. 61, Nos. 3–4, 292–303, 2007.
9. Tabatadze, V., B. Baratashvili, I. Petoev, and R. Zaridze, "Tunnel detection and visualization using the method of auxiliary sources," *2017 XXIInd International Seminar/Workshop on Direct and Inverse Problems of Electromagnetic and Acoustic Wave Theory (DIPED)*, 25–28, 2017.
10. Güner, Ö. F., V. Tabatadze, and S. Eker, "Polyethylene pipeline detection and visualization using the method of auxiliary sources," *2020 International Applied Computational Electromagnetics Society Symposium (ACES)*, 1–2, 2020.
11. Vertiy, A. A., S. Gavrilov, and S. Aksoy, "Imaging of buried objects by microwave tomography method in conditions of low reflection on surface medium," *ICMMT 2000. 2000 2nd International Conference on Microwave and Millimeter Wave Technology Proceedings (Cat. No. 00EX364)*, 615–618, 2000.

12. Tabatadze, V., K. Karaçuha, E. Karaçuha, and R. Zaridze, "A simple approach to determine the buried object under the ground," *2021 IEEE 26th International Seminar/Workshop on Direct and Inverse Problems of Electromagnetic and Acoustic Wave Theory (DIPED)*, 177–180, 2021.
13. Bogdanov, F. G., D. D. Karkashadze, and R. S. Zaridze, "The method of auxiliary sources in electromagnetic scattering problems," *Generalized Multipole Techniques for Electromagnetic and Light Scattering*, 143–172, Elsevier, 1999.
14. Zaridze, R. S., R. Jobava, G. Bit-Banik, D. Karkasbadze, D. P. Economou, and N. K. Uzunoglu, "The method of auxiliary sources and scattered field singularities (caustics)," *Journal of Electromagnetic Waves and Applications*, Vol. 12, No. 11, 1491–1507, 1998.
15. Jeladze, V. B., T. R. Nozadze, V. A. Tabatadze, I. A. Petoev-Darsavelidze, M. M. Prishvin, and R. S. Zaridze, "Electromagnetic exposure study on a human located inside the car using the method of auxiliary sources," *J. Commun. Technol. Electron.*, Vol. 65, 457–464, 2020.
16. Tabatadze, V., K. Karaçuha, E. Veliyev, E. Karaçuha, and R. Zaridze, "The electric field calculation for mobile communication coverage in buildings and indoor areas by using the method of auxiliary sources," *Complexity*, Vol. 2020, 4563859, 2020, doi: 10.1155/2020/4563859.
17. Jeladze, V. B., T. R. Nozadze, V. A. Tabatadze, I. A. Petoev-Darsavelidze, M. M. Prishvin, and R. S. Zaridze, "Electromagnetic exposure study on a human located inside the car using the method of auxiliary sources," *J. Commun. Technol. Electron.*, Vol. 65, No. 5, 457–464, 2020, doi: 10.1134/S1064226920050034.
18. Stratton, J. A., *Electromagnetic Theory*, John Wiley & Sons, 2007.
19. Akdoğan, H., V. Tabatadze, K. Karaçuha, and E. Yaldiz, "Several case studies on electric field distributions for two human bodies inside the car at 3.5 GHz-5G frequency band," *Int. J. Appl. Electromagn. Mech.*, Vol. 67, 507–520, 2021, doi: 10.3233/JAE-210035.
20. Balanis, C. A., *Advanced Engineering Electromagnetics*, John Wiley & Sons, 1999.
21. Tabatadze, V., D. Kakulia, G. Saparishvili, R. Zaridze, and N. Uzunoglou, "Development of a new efficient numerical approach for buried object recognition," *Sens. Imaging*, Vol. 12, Nos. 1–2, 35–56, 2011, doi: 10.1007/s11220-011-0060-7.
22. Balanis, C. A., *Antenna Theory: Analysis and Design*, John Wiley & Sons, 2016.